AGU PUBLICATIONS

Geophysical Research Letters

RESEARCH LETTER
10.1002/2016GL068076

Key Points:
- New approach to quantify eruptive processes combining lightning and umbrella expansion rates from the 2015 Calbuco eruption
- Formation of hazardous pyroclastic density currents signaled by a sharp increase in proximal lightning and slower upwind plume expansion
- Observations and modeling suggest that ice formation above 10 km controlled the propagation of volcanic lightning downwind

Supporting Information:
- Supporting Information S1
- Table S3

Correspondence to:
A. R. Van Eaton,
avaneaton@usgs.gov

Citation:
Van Eaton, A. R., Á. Amigo, D. Bertin, L. G. Mastin, R. E. Giacosa, J. González, O. Valderrama, K. Fontijn, and S. A. Behnke (2016), Volcanic lightning and plume behavior reveal evolving hazards during the April 2015 eruption of Calbuco volcano, Chile, *Geophys. Res. Lett.*, *43*, doi:10.1002/2016GL068076.

Received 2 FEB 2016
Accepted 7 MAR 2016
Accepted article online 11 MAR 2016

Volcanic lightning and plume behavior reveal evolving hazards during the April 2015 eruption of Calbuco volcano, Chile

Alexa R. Van Eaton[1], Álvaro Amigo[2,3], Daniel Bertin[2], Larry G. Mastin[1], Raúl E. Giacosa[4], Jerónimo González[4], Oscar Valderrama[2], Karen Fontijn[5], and Sonja A. Behnke[6]

[1]Cascades Volcano Observatory, U.S. Geological Survey, Vancouver, Washington, USA, [2]Observatorio Volcanológico de los Andes del Sur, Servicio Nacional de Geología y Minería, Temuco, Chile, [3]Centro de Excelencia en Geotermia de los Andes, Universidad de Chile, Santiago, Chile, [4]Delegación Regional Comahue, Servicio Geológico Minero Argentino, General Roca, Río Negro, Argentina, [5]Department of Earth Sciences, University of Oxford, Oxford, UK, [6]Los Alamos National Laboratory, Los Alamos, New Mexico, USA

Abstract Soon after the onset of an eruption, model forecasts of ash dispersal are used to mitigate the hazards to aircraft, infrastructure, and communities downwind. However, it is a significant challenge to constrain the model inputs during an evolving eruption. Here we demonstrate that volcanic lightning may be used in tandem with satellite detection to recognize and quantify changes in eruption style and intensity. Using the eruption of Calbuco volcano in southern Chile on 22 and 23 April 2015, we investigate rates of umbrella cloud expansion from satellite observations, occurrence of lightning, and mapped characteristics of the fall deposits. Our remote sensing analysis gives a total erupted volume that is within uncertainty of the mapped volume ($0.56 \pm 0.28\ km^3$ bulk). Observations and volcanic plume modeling further suggest that electrical activity was enhanced both by ice formation in the ash clouds >10 km above sea level and development of a low-level charge layer from ground-hugging currents.

1. Introduction

Rapid characterization of explosive eruptions is an ongoing challenge to short-term hazards forecasting. In particular, the mass eruption rate has a first-order influence on the accuracy of ash dispersal forecasts, yet is difficult to quantify in near real-time. Despite important advances in the use of weather radar, infrasound, and satellite detection to measure eruptive intensity [*Marzano et al.*, 2013; *Pouget et al.*, 2013; *Ripepe et al.*, 2013], no single technique is universally applicable, especially to remote volcanoes with sparse in situ geophysical instruments. Recently, volcanic lightning has been recognized as a valuable complementary tool [*Behnke and McNutt*, 2014]. With continued expansion and improvement of global networks such as the World Wide Lightning Location Network (WWLLN) [*Lay et al.*, 2004], and deployable lightning mapping arrays [*Behnke et al.*, 2013, 2014], it is increasingly apparent that volcanic lightning could become a crucial part of eruption detection and monitoring operations in the future. With these developments come new questions about the role of lightning in eruption processes. How does volcanic lightning relate to the evolving dynamics of an eruption? And how might it be integrated into conventional data streams, such as satellite detection of volcanic plumes? We investigate these questions in our study of the 2015 eruption of Calbuco volcano in Southern Chile, which produced abundant WWLLN-detected lightning during clear weather (>1100 lightning strokes). The eruption presents a rare opportunity to combine excellent ground observations and tephra deposits with remote sensing data.

On 22 April 2015, Calbuco volcano erupted for the first time in 43 years, with very little warning (<3 h of precursory seismicity). The initial two explosive phases occurred in rapid succession with a ~5.5 h time break in between, producing tephra of andesite composition (57–58% SiO_2; Table S1 in the supporting information). During both events, ash-rich columns rose into the stratosphere, with maximum plume heights reaching 23 km above sea level (asl) in weather radar [*Vidal et al.*, 2015]. Over 6500 people were evacuated within 20 km of the volcano while the ash dispersed in a northeasterly direction across Chile, Argentina and Uruguay, damaging buildings, affecting agriculture, closing airports, and delaying flights. As the event unfolded, clear views from satellite and visual observations shared on social media provided an unusually complete perspective of the eruption columns. A few days later on 30 April a third, smaller eruption began

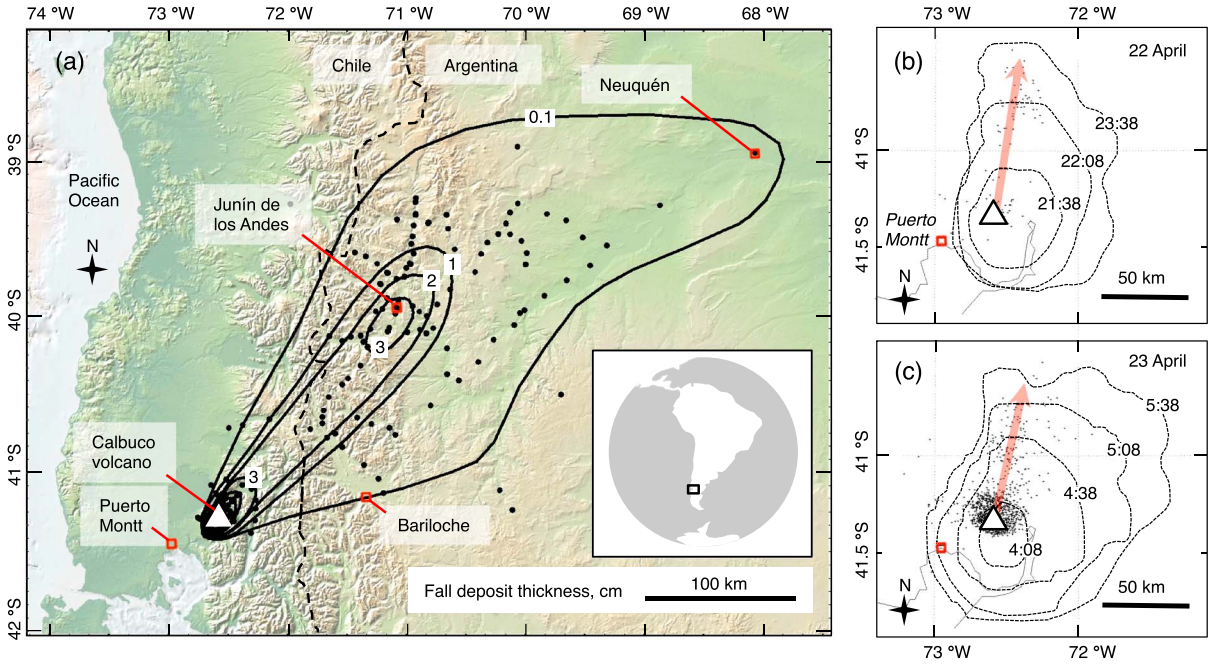

Figure 1. Location of fall deposits, umbrella clouds, and lightning from the 2015 Calbuco eruption. (a) Isopachs of fall deposit thickness in centimeters. Black circles show measurement locations ($n = 163$). Note secondary thickness maximum ~150 km downwind, near the city of Junín de los Andes. Dashed line shows the border between Chile and Argentina. Outlines of the umbrella clouds through time, UTC, from the (b) first and (c) second eruptive phases, derived from thermal infrared satellite images and shown until the umbrella no longer propagates upwind. Grey dots show locations of WWLLN-detected lightning; red arrows show direction of lightning locations with time. White triangles indicate Calbuco volcano. Note that in both phases, the majority of the lightning moved northward (azimuth $\leq 15°$), while the axis of the fall deposit tracked northeast (azimuth 38–45°).

at 16:08 UTC, lasting ~2 h and producing a low ash plume (<4.5 km asl). This event did not generate WWLLN-detected lightning, and its low juvenile content indicates a steam-driven eruption with little involvement of fresh magma. Our study focuses on the first two explosive phases, combining field mapping, satellite and lightning analysis, and seismic observations. The overall aims are to reconstruct the eruptive behavior and consider the implications for providing rapid situational awareness of hazards.

2. Field Observations of the Deposits

The thickness and stratigraphy of the fall deposits were documented at 163 sites out to ~460 km downwind (Figures 1a, S1, and Table S3). Assuming the deposits become exponentially thinner with distance from source [*Fierstein and Nathenson*, 1992], we estimate a total bulk volume of 0.58 km^3, indicating a VEI 4 on the volcanic explosivity index [*Newhall and Self*, 1982]. Uncertainty is likely on the order of 50% (±0.28 km^3) due to the local effects of deposit compaction, wind remobilization, and the plausible range of assumptions associated with the volume calculation [*Sulpizio*, 2005; *Engwell et al*., 2015] (Figure S1). By comparison, the bulk volume estimates of *Romero et al*. [2016] are within uncertainty of our calculations, though somewhat on the lower end. The majority of the fall deposit is from the more energetic second phase, consisting of a lower light-grey to tan and upper dark grey layer (Figure S1). The upper dark grey tephra contains high-density scoria [*Romero et al*., 2016], which is texturally similar to juvenile blocks in the most voluminous pyroclastic density current (PDC) deposits associated with the eruption (bulk volume 0.01–0.05 km^3). There were also PDCs at the end of the first eruptive phase, but the largest occurred in the early hours of 23 April, attaining runout distances of 7–8 km down the Río Blanco (Figure S1a). In the distal fall deposit, a secondary thickness maximum occurred in the region of Junín de los Andes, about 150 km downwind, where residents reported at least 3 cm of freshly fallen ash (Figure 1a). Local observers recorded the ash falling as low-density clusters [see *Herrera*, 2015], suggesting that ash aggregation enhanced sedimentation rates in this area [*Sorem*, 1982; *Taddeucci et al*., 2011].

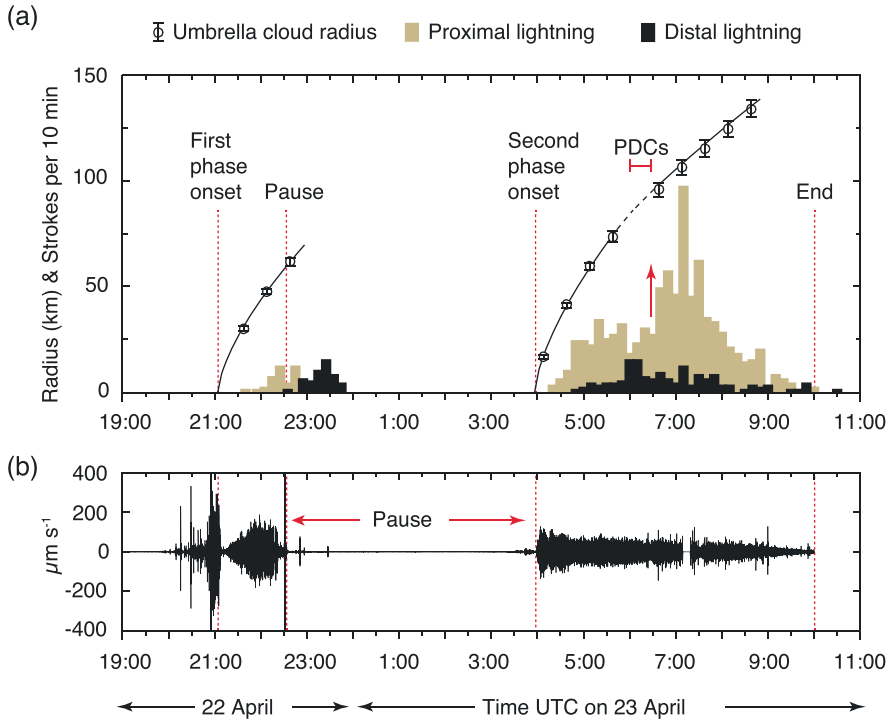

Figure 2. Time series of satellite, lightning, and seismic observations. (a) Symbols show mean and range of umbrella radius, defined by GOES-13 brightness temperatures of −3 and −13°C. Black curves show best fit theoretical expression for umbrella expansion rates using equation (1). WWLLN-detected lightning stroke rates are given in 10 min intervals for proximal (<20 km) and distal lightning (>20 km from volcano). Red lines indicate eruption processes described in text. Note the shift to slower umbrella expansion rates after ~5:30 on 23 April (dashed line) and sharp increase in proximal lightning (red arrow), when we infer formation of significant PDCs. (b) Seismic amplitude filtered between 0.5 and 5 Hz, from station ~3 km from the summit. Gap in seismic data occurs ~7:15 due to temporary lapse in communications.

3. Satellite and Lightning Analysis

During sustained, high-intensity eruptions, the vertical ash column rises to a maximum height and expands outward as an umbrella cloud near the level of neutral buoyancy [*Sparks*, 1986; *Pouget et al*., 2013]. Both ash-producing phases of the Calbuco eruption were recorded by the GOES-13 satellite and were used to calculate umbrella expansion rates (Figures 1b, 1c, S3, S4, and Table S2). Umbrella clouds expand radially as a gravity current, driven by the intrusion of mass and drop in height from the overshooting top of the plume to the level of neutral buoyancy. Growth of the umbrella radius (R) after time (t) since the start of eruption is proportional to the volumetric flow rate (V) of ash, gas, and entrained air injected into the umbrella region (in $m^3\,s^{-1}$). The relationship may be approximated by [*Woods and Kienle*, 1994]

$$R = (3\lambda NV/2\pi)^{1/3} t^{2/3}, \tag{1}$$

where λ is an empirical cloud shape factor, taken as 0.2 after *Suzuki and Koyaguchi* [2009] and N is the Brunt-Väisälä frequency of the atmosphere, calculated here to be $0.014\,s^{-1}$ using the method of *Mastin* [2014]. We fit this equation to the observed umbrella dimensions through time by adjusting the start time and volumetric flow rate V (Figure 2a; Appendix A). The volumetric flow rate into the umbrella relates to the mass eruption rate M (in $kg\,s^{-1}$) and entrainment of ambient air, according to the following [*Morton et al*., 1956; *Sparks*, 1986]:

$$M \approx \left(VN^{5/8}/C\sqrt{k_e}\right)^{4/3}, \tag{2}$$

where k_e is the radial entrainment coefficient of the rising plume, taken as 0.1, and C is a proportionality constant, assumed to be $1\times10^4\,m^3\,kg^{-3/4}\,s^{-7/8}$ for midlatitude eruptions [*Suzuki and Koyaguchi*, 2009; *Mastin et al*., 2014]. The timing and location of lightning strokes were obtained from the WWLLN Global

Table 1a. Characteristics of Individual Phases of the Calbuco Eruption From 22-23 April 2016[a]

		Individual Eruptive Phases	
Parameter	Method(s)	Phase 1	Phase 2
Eruption onset (UTC)	umbrella	22 Apr 21:04	23 Apr 03:54
	seismicity	22 Apr 21:04	23 Apr 04:00
Eruption end (UTC)	visual obs.	22 Apr 22:35	23 Apr 10:00
Duration (h:mm)	umbrella, visual obs.	1:31	6:14
Umbrella height (km asl)	satellite	14.5–15.5	16.9–17.3
MER (kg s^{-1})	umbrella	6.0×10^6	$9.5–6.6 \times 10^6$
Detected lightning strokes (#)	WWLLN	93	1,016
Lightning delay (min)	WWLLN	37	30
Last stroke <10 km (UTC)	WWLLN	22 Apr 22:58	23 Apr 10:08

[a]MER, mass eruption rate; values for second phase given before and after the inferred shift in eruption style between 5:38 and 6:38 UTC. WWLLN, World Wide Lightning Location Network. Umbrella height indicates the top of the umbrella clouds from satellite images, although it is noted that weather radar detected overshooting tops at least 23 km asl during both phases [*Vidal et al.*, 2015]. Lightning delay indicates time gap between eruption onset (umbrella method) and the first WWLLN-detected lightning stroke. Last stroke indicates timing of final stroke detected within 10 km of volcano.

Volcanic Lightning Monitor [*Ewert et al.*, 2010], which detects 3–30 kHz radio waves (Figures 1b and 1c). WWLLN preferentially detects cloud-to-ground lightning, which accounts for about 2/3 of detected strokes [*Hutchins et al.*, 2012].

4. Insights Into Eruption Dynamics

Umbrella cloud growth from both eruptive phases is compared with WWLLN stroke rates and seismic amplitude in Figure 2. Times are given in UTC (note that local time is UTC–3 h). During the first eruptive phase on 22 April, WWLLN detected 93 lightning strokes moving progressively northward from Calbuco volcano out to 67 km. The best fit umbrella growth curve in Figure 2a gives a start time of 21:04 UTC, which is consistent with the seismic onset (Table 1a). In satellite, the umbrella stops expanding upwind by 22:38 UTC (Figure 1 b), followed by a decline in proximal strokes (<20 km from the volcano). This behavior is consistent with an end time of ~22:35 UTC determined from visual and seismic observations (Figure 2).

During the second eruptive phase on 23 April 2015, WWLLN detected 1016 lightning strokes up to 113 km from the volcano—more than 10 times the number of strokes from the first phase. This event occurred at night, and observers documented abundant lightning in the vertical column and downwind cloud. Using a best fit umbrella growth curve based on the first four satellite images, we derive an eruption start time of about 3:54 UTC, which is within a few minutes of the seismic onset. This cloud expands more rapidly than the first, indicating a ~50% greater eruption rate (Table 1a). Interestingly, the umbrella stops expanding upwind sometime between 5:38 and 6:38 UTC (Figure S4), despite an ongoing eruption and no significant changes in the background wind field (Figures 3a and S2). The end of upwind spreading, followed by recession of the cloud, suggests a lower mass flux supplied to the umbrella (Table 1a). Around the same time, proximal strokes increase sharply, peak at 7:20 UTC and decline thereafter, with the final stroke <10 km from the volcano occurring at 10:05 UTC. The waning electrical activity is consistent with direct observations that the eruption continued at a low level until ~10:00 UTC.

Table 1b. Total Erupted Volume and Time-Averaged MER of the Calbuco Eruption[a]

Parameter	Method	Total Eruption (Phases 1 and 2)
Erupted volume, bulk (km^3)	umbrella	0.25
	fall deposit	0.56 ± 0.28
Erupted volume, DRE (km^3)	umbrella	0.08
	fall deposit	0.18 ± 0.09
Time-averaged MER (kg s^{-1})	fall deposit	0.8×10^6 to 2.4×10^7

[a]Volume calculations assume magma density 2500 kg m^3 and bulk deposit density 800 kg m^3. Time-averaged mass eruption rate is derived from total erupted mass (from fall deposit mapping) and total duration of eruption. DRE, dense-rock equivalent. MER, mass eruption rate.

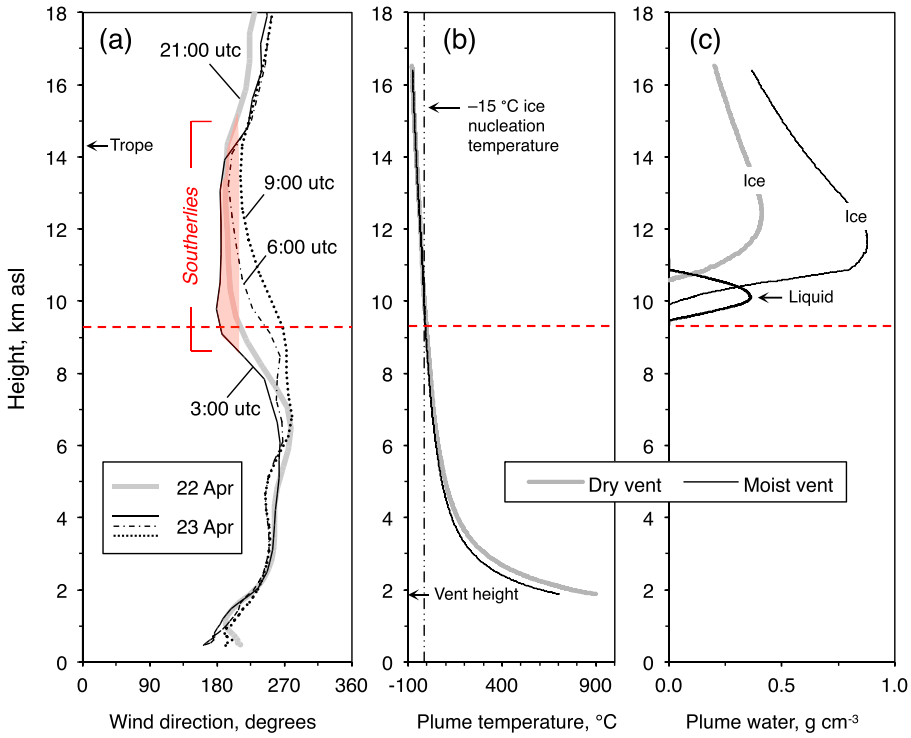

Figure 3. Atmospheric wind profiles and 1-D plume model results. (a) Background winds over Calbuco volcano from the NOAA 0.5° GDAS model, indicating direction from which the wind is coming. *Trope*, cold-point tropopause. (b) Modeled temperature of the volcanic plume, assuming dry or moist conditions at vent (up to 5 wt % surface water ingested at the eruptive source). Vertical dash-dotted line shows the −15°C ice nucleation temperature for volcanic ash (see Appendix B). (c) Modeled abundance and phase of water inside the volcanic plume. Dry vent conditions lead to sparse liquid water contents (not visible on this scale). Note that heights of liquid water and ice formation in the plume (red dashed line) correspond to southerly winds in the background atmosphere.

In previous studies, increased lightning rates have been linked to the expanding size of the cloud [*Williams*, 1985; *Behnke and Bruning*, 2015]. However, the dramatic rise in proximal lightning stroke rates detected after ~6:30 UTC on 23 April reflects an impulsive change at the source, rather than gradually increasing cloud volume. We suspect that the lightning was triggered by PDCs from Calbuco volcano (Figure 2a). Low-level ash clouds near the PDCs would introduce a new atmospheric charge layer capable of triggering cloud-to-ground lightning [*Hoblitt*, 1994]. Direct visual observations of the nighttime PDCs are lacking, due in part to their northeast flow direction, out of view from the populated areas. Yet the shift in eruption style is evident from three key observations: (1) increased stroke rates are seen only in proximal lightning, suggesting an origin near the volcano, (2) at the same time, upwind cloud expansion ends, indicating a more sluggish flux into the high plume, and (3) the stratigraphic shift from light to dark grey tephra occurs partway through the deposits of the second phase (Figure S1, also recognized by *Romero et al*. [2016]). The color change corresponds to a greater abundance of high-density clasts that are texturally correlated to the PDCs. When an eruption column undergoes partial collapse, it transports mass into both a buoyant plume and ground-hugging PDCs [*Neri et al*., 2002; *Van Eaton et al*., 2012]. We suspect that during this time, when the eruption was producing dark grey (high-density) tephra, some portion rose vertically into the high plume while the rest partitioned into PDCs. Low-level clouds lofted from the PDCs may have accumulated as fall deposits in the distal area without rising all the way into the umbrella cloud, such as those that occurred during the 1980 eruption of Mount St. Helens [*Carey et al*., 1990]. This is consistent with the larger erupted volume calculated from our fall deposit mapping compared to the umbrella expansion method (although both are within uncertainty).

5. What Caused the Volcanic Lightning?

Both eruptive phases produced abundant lightning, yet the WWLLN-detected strokes drifted mainly to the north rather than following the dispersal axis of the fall deposits (Figure 1). What caused the electrical

activity during this eruption, and why did the lightning decouple from the bulk of the cloud? To address these questions, we used the 1-D model *Plumeria* [*Mastin*, 2007, 2014] to investigate the thermodynamics of the eruption column. *Plumeria* calculates time-averaged, mean properties of a steady state volcanic plume, accounting for the effects of crosswinds, entrainment of atmospheric moisture, and the formation of liquid water and ice. Aggregation processes are not resolved. We added the approach of *Schill et al*. [2015] to account for heterogeneous ice nucleation in the presence of volcanic ash (Appendix B). The model was initialized with an atmospheric profile of temperature, humidity, and wind from 3–6 UTC on 23 April (Figures 3a and S2), and an eruption rate of 1×10^7 kg s^{-1} consistent with our measurements.

Although all volcanic plumes contain some amount of water from the magma (generally 2–6 wt %) [*Plank et al*., 2013] and entrained from the atmosphere [*Glaze et al*., 1997], plume behavior is also sensitive to the amount of water incorporated from the Earth's surface [*Koyaguchi and Woods*, 1996; *Van Eaton et al*., 2012]. To examine these effects, we explored dry and moist conditions at the volcanic source [*Woodhouse and Behnke*, 2014]. The "dry vent" scenario assumes no interaction with the hydrological system and includes only magmatic water in the erupted mixture (5 wt % is assumed)—although water is also entrained from the atmosphere during ascent. The "moist vent" scenario adds a small but significant amount of cooler surface water to the plume (an additional 5 wt %). There is no reason to suspect that the Calbuco eruption plumes were phreatomagmatic in the traditional sense (for example, no accretionary lapilli were observed in the deposits) [*Houghton et al*., 2015]. However, some amount of surface water interaction cannot be ruled out for two reasons: (1) the existence of a summit glacier ~0.02 km^3 prior to the eruption [*Pelto*, 2015], and (2) vigorous fumarolic activity, including the steam-driven eruption on 30 April 2015, indicating that water was circulating in the system even a few days after the climactic events. Adding an additional 5 wt % surface water in the "moist vent" scenario (Figures 3b and 3c) represents a reasonable upper limit in this case [see *Houghton et al*., 2000]. Even such modest degrees of surface water interaction are important to consider because they can significantly impact the dynamics and microphysics of volcanic plumes [*Van Eaton et al*., 2012, 2015].

Modeling results suggest that liquid water and ice formed above 9–10 km asl (Figure 3c). This height corresponds to a change in wind direction toward the north (Figure 3a). In other words, upper level winds were blowing the fine-grained, icy tops of the plumes northward, in the direction of lightning movement.

Our results provide clues about the nature of plume electrification. First, some interaction between fine ash, liquid water and ice is likely to have occurred in the upper troposphere. However, it is unlikely that riming and hail-forming processes [cf. *Van Eaton et al*., 2015] played a volumetrically significant role, given the lack of evidence for wet ash aggregation in the proximal deposits. Second, the colocation of ice formation and southerly winds (Figure 3) suggests that ice was involved in the lightning that drifted northward from Calbuco volcano. We infer that the largest particles were transported at lower levels to the northeast, forming the bulk of the fall deposits. Meanwhile, the smaller particles at the top of the plume (fine ash and cloud ice) moved north, generating lightning in the distal cloud many tens of kilometers downwind of the volcano [cf. *Kuhlman et al*., 2009].

These findings support the concept of a *dirty thunderstorm* charging mechanism during high-intensity eruptions [*Williams and McNutt*, 2005], which stems from the idea that regular thunderstorms become electrified during ice collisions in the mixed phase region of vertical updrafts [*Deierling et al*., 2008]. Without ice, there is no lightning in meteorological clouds. However, not all volcanic lightning is analogous to a dirty thunderstorm [*Cimarelli et al*., 2013; *Behnke et al*., 2014]. Volcanic ash enters the atmospheric plume "precharged" from fragmentation and particle-particle collisions near the vent [*James et al*., 2008]. Therefore, even very small eruptions produce low-energy discharges in the absence of ice, referred to as *vent* or *near-vent lightning* [*Thomas et al*., 2010]. Ice likely plays a role in enhancing electrification during larger eruptions that produce large-scale *plume lightning* (intracloud or cloud-to-ground discharges a few kilometers to tens of kilometers in extent), which develops some minutes to tens of minutes after eruption onset [*Behnke et al*., 2013]. In the case of the Calbuco eruption, we suspect that the WWLLN-detected lightning falls into this category, consistent with a ~30 min detection delay for both eruptive phases (Table 1a). Furthermore, we propose that the electrical activity was enhanced both by ice-forming processes and creation of a low-level charge layer from PDCs.

6. Conclusions

We have demonstrated that changes in the lightning activity and satellite-detected plume dynamics may be used to infer key aspects of eruption behavior, including the mass eruption rate, volume, start time, and duration—all of which are necessary parameters for ash dispersal modeling. Our estimates of erupted volume and mass eruption rate using the umbrella expansion technique are within uncertainty of the fall deposit mapping (Table 1b). However, it is important to note that umbrella-derived volumes only reflect the mass flux into the high-level plume, neglecting contributions from low-level clouds or PDCs. Therefore such estimates should be considered minimum values for the fall deposits and other eruptive products as a whole. Volcanic lightning also offers some promising insights into the eruptive activity. Our findings suggest that a simultaneous increase in proximal lightning and diminished upwind expansion of the umbrella cloud may signal formation of hazardous, ground-hugging PDCs. In the case of the 2015 Calbuco eruption, PDCs exerted an important influence on the intensity of proximal lightning ($<$20 km from volcano), whereas the movement of distal lightning correlates to ice particles carried downwind in the high plume ($>$10 km asl). An observed delay of 30–37 min between eruption onset and WWLLN-detected lightning (Table 1a) indicates that this kind of large-scale plume lightning can sometimes take time to develop, which should be taken into account during eruption detection. We conclude that satellite observations and lightning detection offer widely accessible tools to monitor eruptive activity in near real-time, particularly high-intensity eruptions that sustain vertical columns well above the local freezing level. This approach is especially valuable in the case of remote volcanoes that lack ground-based monitoring instruments or have local networks with restricted data access.

Appendix A: Calculating Start Time and Mass Eruption Rate From Umbrella Expansion

Infrared satellite images from GOES-13 were analyzed within time periods of ongoing eruption, before the umbrella began to separate from the vent (Figures S3 and S4). In each image, the edge of the umbrella was outlined using Unidata's IDV software [*Unidata*, 2015]. Brightness temperatures of −3°C and −13°C were used to define the maximum and minimum dimensions, respectively. Images were cropped to remove background meteorological clouds and processed using ImageJ software [*Schneider et al*., 2012] to determine the area of each umbrella cloud contour (km^2). Where clouds from the first and second phases began to merge (Figures S4g and S4j), the outer contours were extrapolated by hand; inner contours were unaffected. Dimensions are reported as the radius of an equivalent circle in Figure 2a and Table S2 (mean and range).

Next, equation (1) was fit to the umbrella data on a plot of radius versus time by adjusting the start time (t_0) and volumetric flow rate (V) until the theoretical curve matched the observed cloud dimensions. For the second eruptive phase, only the first four data points were used to calculate the eruption onset. This is due to the change in cloud morphology and apparent expansion rate after 5:38–6:38 UTC (Figures S4e and S4f). Beyond this point, a new V and (arbitrary) t_0 were used to fit the observations. Once the values of V were converted to mass eruption rate using equation (2), erupted volumes for each phase were calculated using the eruption durations reported in Table 1a. For simplicity, we assumed that the shift in eruption rate occurred at 6:08 UTC, halfway between the two satellite observations in Figures S4e and S4f.

As in *Sparks* [1986] and *Pouget et al*. [2013], this method makes the simplifying assumption that growth in umbrella radius is roughly proportional to $t^{2/3}$ over the entire eruption. In a more detailed study, *Pouget et al*. [2016] found that this relationship may change over time due to changes in the flow regime of the gravity current. However, the $t^{2/3}$ approximation was valid within uncertainty for the majority of cases investigated. In the case of the second eruptive phase from Calbuco volcano, it is possible there was a change in umbrella flow regime after 5:38–6:38 UTC. However, the independent lines of evidence for a shift in umbrella morphology (change in upwind stagnation point), lightning intensity, fall deposit stratigraphy, and radar observations [*Vidal et al*., 2015] are consistent with a change in eruption dynamics at source.

Appendix B: Modeled Ice Formation

We have updated the microphysical formulation in the 1-D model *Plumeria* to include recent experimental work by *Schill et al*. [2015] constraining the nucleation of ice on volcanic ash. Combining their empirical curve

(dashed line from Figure 8 of Schill et al.) and their equation (2), the relationship between temperature (T) in °C and the frozen fraction (FF) of ash-laden water is described using

$$\mathrm{FF} = 1 - \exp\left[-\mathrm{SA}_p \times M_p \times 100 \exp\left(-0.03T^2 - 1.87T - 22.05\right)\right], \quad \text{(B1)}$$

where M_p is the mass of each particle, assuming a mean diameter of 63 μm and density of 2.6 g cm^{-3} and SA_p is particle surface area, taken as 6.3 m^2 g^{-1} from the measurements of *Schill et al*. [2015]. Under these assumptions, ice begins to form in the plume at −15°C and coexists with liquid water until total glaciation at −23°C.

Acknowledgments

The authors wish to thank Bob Holzworth and the World Wide Lightning Location Network (http://wwlln.net), a collaboration among over 50 universities and institutions, for providing the lightning location data used in this paper. James Muirhead, Gregory Schill, Hans Schwaiger, Heather Wright, Dave Schneider, Sebastian García, Lizette Bertin, and Mauricio Mella are thanked for assistance and discussion. A. Van Eaton acknowledges a U.S. Geological Survey Mendenhall Postdoctoral Fellowship. K. Fontijn acknowledges support by NERC urgency grant NE/N007271/1, and assistance by David Pyle, Jonathan Hunt, Romina Daga, Alexandre Corgne, Eduardo Jaramillo, and students from the Universidad Austral de Chile, Valdivia. This work is a contribution from the Fondap Conicyt #15090013 project "Centro de Excelencia en Geotermia de los Andes (CEGA)." Reviewers John Ewert, Earle R. Williams, and Magnús T. Gudmundsson are thanked for valuable comments. GeoMapApp and Unidata's IDV were used in the production of Figure 1. Data used in this study are listed in the references, tables, and supporting information.

References

Behnke, S. A., and E. C. Bruning (2015), Changes to the turbulent kinematics of a volcanic plume inferred from lightning data, *Geophys. Res. Lett.*, *42*, 4232–4239, doi:10.1002/2015GL064199.

Behnke, S. A., and S. R. McNutt (2014), Using lightning observations as a volcanic eruption monitoring tool, *Bull. Volcanol.*, *76*, doi:10.1007/s00445-014-0847-1.

Behnke, S. A., R. J. Thomas, S. R. McNutt, D. J. Schneider, P. R. Krehbiel, W. Rison, and H. E. Edens (2013), Observations of volcanic lightning during the 2009 eruption of Redoubt Volcano, *J. Volcanol. Geotherm. Res.*, *259*, 214–234, doi:10.1016/j.jvolgeores.2011.12.010.

Behnke, S. A., R. J. Thomas, H. E. Edens, P. R. Krehbiel, and W. Rison (2014), The 2010 eruption of Eyjafjallajökull: Lightning and plume charge structure, *J. Geophys. Res. Atmos.*, *119*, 833–859, doi:10.1002/2013JD020781.

Carey, S., H. Sigurdsson, J. E. Gardner, and W. Criswell (1990), Variations in column height and magma discharge during the May 18, 1980 eruption of Mount St. Helens, *J. Volcanol. Geotherm. Res.*, *43*, 99–112.

Cimarelli, C., M. A. Alatorre-Ibargüengoitia, U. Kueppers, B. Scheu, and D. B. Dingwell (2013), Experimental generation of volcanic lightning, *Geology*, *42*, 79–82, doi:10.1130/g34802.1.

Deierling, W., W. A. Petersen, J. Latham, S. Ellis, and H. J. Christian (2008), The relationship between lightning activity and ice fluxes in thunderstorms, *J. Geophys. Res.*, *113*, D15210, doi:10.1029/2007JD009700.

Engwell, S. L., W. P. Aspinall, and R. S. Sparks (2015), An objective method for the production of isopach maps and implications for the estimation of tephra deposit volumes and their uncertainties, *Bull. Volcanol.*, *77*, 61, doi:10.1007/s00445-015-0942-y.

Ewert, J. W., R. H. Holzworth, and A. K. Diefenbach (2010), Global detection of explosive volcanic eruptions with the World Wide Lightning Location Network (WWLLN) and application to aviation safety, Abstract AE31A-04 presented at 2010 Fall Meeting, AGU, San Francisco, Calif., 13–17 Dec.

Fierstein, J., and M. Nathenson (1992), Another look at the calculation of fallout tephra volumes, *Bull. Volcanol.*, *54*, 156–167, doi:10.1007/BF00278005.

Glaze, L. S., S. M. Baloga, and L. Wilson (1997), Transport of atmospheric water vapor by volcanic eruption columns, *J. Geophys. Res.*, *102*, 6099–6108, doi:10.1029/96JD03125.

Herrera, N. (2015), Juninde Los Andes Bajo Ceniza. [Available at https://www.youtube.com/watch?v=Qa_ZW4oXHJI, Accessed 31 Jan 2016.]

Hoblitt, R. P. (1994), An experiment to detect and locate lightning associated with eruptions of Redoubt Volcano, *J. Volcanol. Geotherm. Res.*, *62*, 499–517, doi:10.1016/0377-0273(94)90049-3.

Houghton, B., J. D. L. White, and A. R. Van Eaton (2015), Phreatomagmatic and related eruption styles, in *The Encyclopedia of Volcanoes*, edited by H. Sigurdsson et al., pp. 537–552, Academic Press, San Diego, Calif.

Houghton, B. F., C. J. N. Wilson, R. T. Smith, and J. S. Gilbert (2000), Phreatoplinian eruptions, in *The Encyclopedia of Volcanoes*, edited by H. Sigurdsson et al., pp. 513–525, Academic Press, San Diego, Calif.

Hutchins, M. L., R. H. Holzworth, J. B. Brundell, and C. J. Rodger (2012), Relative detection efficiency of the World Wide Lightning Location Network, *Radio Sci.*, *47*, RS6005, doi:10.1029/2012RS005049.

James, M. R., L. Wilson, S. J. Lane, J. S. Gilbert, T. A. Mather, R. G. Harrison, and R. S. Martin (2008), Electrical charging of volcanic plumes, *Space Sci. Rev.*, *137*, 399–418, doi:10.1007/s11214-008-9362-z.

Koyaguchi, T., and A. W. Woods (1996), On the formation of eruption columns following explosive mixing of magma and surface water, *J. Geophys. Res.*, *101*, 5561–5574, doi:10.1029/95JB01687.

Kuhlman, K. M., D. R. MacGorman, M. I. Biggerstaff, and P. R. Krehbiel (2009), Lightning initiation in the anvils of two supercell storms, *Geophys. Res. Lett.*, *36*, L07802, doi:10.1029/2008GL036650.

Lay, E. H., R. H. Holzworth, C. J. Rodger, J. N. Thomas, O. Pinto Jr., and R. L. Dowden (2004), WWLL global lightning detection system: Regional validation study in Brazil, *Geophys. Res. Lett.*, *31*, L03102, doi:10.1029/2003GL018882.

Marzano, F. S., E. Picciotti, M. Montopoli, and G. Vulpiani (2013), Inside volcanic clouds: Remote sensing of ash plumes using microwave weather radars, *Bull. Am. Meteorol. Soc.*, *94*, 1567–1586, doi:10.1175/bams-d-11-00160.1.

Mastin, L. G. (2007), A user-friendly one-dimensional model for wet volcanic plumes, *Geochem. Geophys. Geosyst.*, *8*, Q03014, doi:10.1029/2006GC001455.

Mastin, L. G. (2014), Testing the accuracy of a 1-D volcanic plume model in estimating mass eruption rate, *J. Geophys. Res. Atmos.*, *119*, 2474–2495, doi:10.1002/2013JD020604.

Mastin, L. G., A. R. Van Eaton, and J. B. Lowenstern (2014), Modeling ash fall distribution from a Yellowstone supereruption, *Geochem. Geophys. Geosyst.*, *15*, 3459–3475, doi:10.1002/2014GC005469.

Morton, B. R., G. I. Taylor, and J. S. Turner (1956), Turbulent gravitational convection from maintained and instantaneous sources, *Proc. R. Soc. London, Ser. A*, *234*, 1–23, doi:10.1098/rspa.1956.0011.

Neri, A., A. Di Muro, and M. Rosi (2002), Mass partition during collapsing and transitional columns by using numerical simulations, *J. Volcanol. Geotherm. Res.*, *115*, 1–18, doi:10.1016/s0377-0273(01)00304-3.

Newhall, C. G., and S. Self (1982), The volcanic explosivity index (VEI): An estimate of explosive magnitude for historical volcanism, *J. Geophys. Res.*, *87*, 1231–1238, doi:10.1029/JC087iC02p01231.

Pelto, M. (2015), Calbuco Volcano Glaciers, Chile, AGU Blog: From a Glacier's Perspective. [Available at http://blogs.agu.org/fromaglacierperspective/2015/04/25/calbuco-volcano-glaciers-chile/, accessed September 2015.]

Plank, T., K. A. Kelley, M. M. Zimmer, E. H. Hauri, and P. J. Wallace (2013), Why do mafic arc magmas contain ~4 wt% water on average?, *Earth Planet. Sci. Lett.*, *364*, 168–179, doi:10.1016/j.epsl.2012.11.044.

Pouget, S., M. Bursik, P. Webley, J. Dehn, and M. Pavolonis (2013), Estimation of eruption source parameters from umbrella cloud or downwind plume growth rate, *J. Volcanol. Geotherm. Res.*, *258*, 100–112, doi:10.1016/j.jvolgeores.2013.04.002.

Pouget, S., M. Bursik, C. G. Johnson, A. J. Hogg, J. C. Phillips, and R. S. J. Sparks (2016), Interpretation of umbrella cloud growth and morphology: Implications for flow regimes of short-lived and long-lived eruptions, *Bull. Volcanol.*, *78*, 1–19, doi:10.1007/s00445-015-0993-0.

Ripepe, M., C. Bonadonna, A. Folch, D. Delle Donne, G. Lacanna, E. Marchetti, and A. Höskuldsson (2013), Ash-plume dynamics and eruption source parameters by infrasound and thermal imagery: The 2010 Eyjafjallajökull eruption, *Earth Planet. Sci. Lett.*, *366*, 112–121, doi:10.1016/j.epsl.2013.02.005.

Romero, J. E., et al. (2016), Eruption dynamics of the 22–23 April 2015 Calbuco volcano (Southern Chile): Analyses of tephra fall deposits, *J. Volcanol. Geotherm. Res.*, *317*, 15–29, doi:10.1016/j.jvolgeores.2016.02.027.

Schill, G. P., K. Genareau, and M. A. Tolbert (2015), Deposition and immersion-mode nucleation of ice by three distinct samples of volcanic ash, *Atmos. Chem. Phys.*, *15*, 7523–7536, doi:10.5194/acp-15-7523-2015.

Schneider, C. A., W. S. Rasband, and K. W. Eliceiri (2012), NIH image to ImageJ: 25 years of image analysis, *Nat. Methods*, *9*, 671–675.

Sorem, R. K. (1982), Volcanic ash clusters: Tephra rafts and scavengers, *J. Volcanol. Geotherm. Res.*, *13*, 63–71.

Sparks, R. S. J. (1986), The dimensions and dynamics of volcanic eruption columns, *Bull. Volcanol.*, *48*, 3–15, doi:10.1007/BF01073509.

Sulpizio, R. (2005), Three empirical methods for the calculation of distal volume of tephra-fall deposits, *J. Volcanol. Geotherm. Res.*, *145*, 315–336, doi:10.1016/j.jvolgeores.2005.03.001.

Suzuki, Y. J., and T. Koyaguchi (2009), A three-dimensional numerical simulation of spreading umbrella clouds, *J. Geophys. Res.*, *114*, B03209, doi:10.1029/2007JB005369.

Taddeucci, J., P. Scarlato, C. Montanaro, C. Cimarelli, E. Del Bello, C. Freda, D. Andronico, M. T. Gudmundsson, and D. B. Dingwell (2011), Aggregation-dominated ash settling from the Eyjafjallajökull volcanic cloud illuminated by field and laboratory high-speed imaging, *Geology*, *39*, 891–894, doi:10.1130/g32016.1.

Thomas, R. J., S. R. McNutt, P. R. Krehbiel, W. Rison, G. Aulich, H. E. Edens, G. Tytgat, and E. Clark (2010), Lightning and electrical activity during the 2006 eruption of Augustine Volcano, *U.S. Geol. Surv. Prof. Pap.*, *1769*, 579–608.

Unidata (2015), Integrated Data Viewer (IDV) version 5.1u2 [software], UCAR/Unidata, Boulder, Colo., doi:10.5065/D6RN35XM.

Van Eaton, A. R., M. Herzog, C. J. N. Wilson, and J. McGregor (2012), Ascent dynamics of large phreatomagmatic eruption clouds: The role of microphysics, *J. Geophys. Res.*, *117*, B03203, doi:10.1029/2011JB008892.

Van Eaton, A. R., L. G. Mastin, M. Herzog, H. F. Schwaiger, D. J. Schneider, K. L. Wallace, and A. B. Clarke (2015), Hail formation triggers rapid ash aggregation in volcanic plumes, *Nat. Commun.*, *6*, 7860, doi:10.1038/ncomms8860.

Vidal, L., S. Nesbitt, P. Salio, S. Osores, C. Farias, A. Rodriguez, J. Serra, and G. Caranti (2015), C-band dual-polarization observations of a massive volcanic eruption in South America, paper presented at 37th Conference on Radar Meteorology, Am. Meteorol. Soc., Norman, Okla., 14–18 Sept.

Williams, E. R. (1985), Large-scale charge separation in thunderclouds, *J. Geophys. Res.*, *90*, 6013–6025, doi:10.1029/JD090iD04p06013.

Williams, E. R., and S. R. McNutt (2005), Total water contents in volcanic eruption clouds and implications for electrification and lightning, in *Recent Progress in Lightning Physics*, edited by C. Pontikis, pp. 81–94, Research Signpost Publishing, Kerala, India.

Woodhouse, M. J., and S. A. Behnke (2014), Charge structure in volcanic plumes: A comparison of plume properties predicted by an integral plume model to observations of volcanic lightning during the 2010 eruption of Eyjafjallajökull, Iceland, *Bull. Volcanol.*, *76*, doi:10.1007/s00445-014-0828-4.

Woods, A. W., and J. Kienle (1994), The dynamics and thermodynamics of volcanic clouds; theory and observations from the 15 and 21 April 1990 eruptions of Redoubt Volcano, Alaska, *J. Volcanol. Geotherm. Res.*, *62*, 273–299.